JOURNAL OF APPLIED PHYSICS **117**, 205301 (2015)

Hydrogenated indium oxide window layers for high-efficiency Cu(In,Ga)Se_2 solar cells

Timo Jäger,[1,a)] Yaroslav E. Romanyuk,[1] Shiro Nishiwaki,[1] Benjamin Bissig,[1] Fabian Pianezzi,[1] Peter Fuchs,[1] Christina Gretener,[1] Max Döbeli,[2] and Ayodhya N. Tiwari[1]
[1]*Empa – Swiss Federal Laboratories for Materials Science and Technology, Laboratory for Thin Films and Photovoltaics, Überlandstrasse 129, 8600 Dübendorf, Switzerland*
[2]*ETH Zürich, Swiss Federal Institute of Technology, Laboratory of Ion Beam Physics, Otto-Stern-Weg 5, 8093 Zürich, Switzerland*

(Received 7 April 2015; accepted 9 May 2015; published online 22 May 2015)

High mobility hydrogenated indium oxide is investigated as a transparent contact for thin film Cu(In,Ga)Se_2 (CIGS) solar cells. Hydrogen doping of In_2O_3 thin films is achieved by injection of H_2O water vapor or H_2 gas during the sputter process. As-deposited amorphous In_2O_3:H films exhibit a high electron mobility of ~50 cm^2/Vs at room temperature. A bulk hydrogen concentration of ~4 at. % was measured for both optimized H_2O and H_2-processed films, although the H_2O-derived film exhibits a doping gradient as detected by elastic recoil detection analysis. Amorphous IOH films are implemented as front contacts in CIGS based solar cells, and their performance is compared with the reference ZnO:Al electrodes. The most significant feature of IOH containing devices is an enhanced open circuit voltage (V_{OC}) of ~20 mV regardless of the doping approach, whereas the short circuit current and fill factor remain the same for the H_2O case or slightly decrease for H_2. The overall power conversion efficiency is improved from 15.7% to 16.2% by substituting ZnO:Al with IOH (H_2O) as front contacts. Finally, stability tests of non-encapsulated solar cells in dry air at 80 °C and constant illumination for 500 h demonstrate a higher stability for IOH-containing devices. © *2015 AIP Publishing LLC*. [http://dx.doi.org/10.1063/1.4921445]

I. INTRODUCTION

Among all polycrystalline thin film photovoltaic (PV) technologies, Chalcopyrite Cu(In,Ga)Se_2 (CIGS) based solar cells show currently the highest power conversion efficiency of 21.7%.[1] As transparent front contacts in CIGS solar cells, aluminum doped zinc oxide (AZO)[2–5] is generally used, which is heavily doped in order to achieve the necessary conductance exhibiting an electron mobility below 30 cm^2/Vs. Optical losses in state-of-the-art AZO contacts are still responsible for about 3% of the theoretical current limit,[6] and the resulting parasitic free carrier absorption in the infrared (IR) region is even more severe in large-area modules, where thicker transparent conductive oxide (TCO) layers are required. Additionally, an elaborated encapsulation for solar modules is required to withstand damp-heat tests due to the relatively low corrosion stability of AZO.[7]

TCOs as front electrodes with matched work function and increased transparency are needed to further enhance the performance of CIGS solar cells. Numerous TCOs have been investigated including $ZnO_{1-x}S_x$:Al,[8] $Zn_{1-x}Mg_xO$:Al,[9] ZnO:B,[10] indium tin oxide (ITO),[11] and also high mobility TCOs such as In_2O_3:Mo and In_2O_3:Ti.[10] Regarding the photovoltaic performance stability, amorphous InZnO implemented in CIGS solar cells exhibits an excellent performance under damp heat condition.[12,13] The amorphous structure of metal oxides has already enabled new possibilities for device fabrication due to their particular features—shock resistance,[14] high aspect ratio for etching and thus easy patterning,[15] uniform film coverage,[16] low deposition temperature,[17] surface smoothness, and thermal stability.[18]

Combining high mobility and amorphous film growth, Koida *et al*. developed hydrogenated In_2O_3 (IOH) by adding small amounts of water vapor during the sputter process.[17,19,20] The effective doping of hydrogen as shallow donors in indium oxide was investigated in detail by density functional theory.[21–23] Owing to its excellent properties, IOH has been implemented in several solar cell technologies including microcrystalline Si,[24,25] silicon hetero-junction,[25,26] and tandem micromorph thin-film silicon solar cells.[27] Scherg-Kurmes *et al*. tested IOH as the front contact in CIGS solar cells which yielded an increased short circuit current (J_{SC}), but their devices suffered from unexpected losses in open circuit voltage (V_{OC}) and fill factor (*FF*).[28] Here, we present a systematic investigation of amorphous In_2O_3:H (a-IOH) layers deposited with two different approaches and demonstrate that a comparable photovoltaic performance can be obtained for IOH and AZO based devices. Importantly, IOH devices exhibit a higher V_{OC} and photovoltaic performance stability in heat exposure.

II. EXPERIMENTAL DETAILS

Hydrogenated indium oxide (In_2O_3:H) layers are grown in a high vacuum sputtering system (AJA Intl.) by RF sputtering of ceramic In_2O_3 (99.99%) targets in a mixed Ar/O_2 atmosphere without intentional heating. The system was equipped with mass flow controllers (MFCs) for multiple gas injection and 5.08 cm (2 in.) planar targets mounted on

a)Author to whom correspondence should be addressed. Electronic mail: timo.jaeger@empa.ch

magnetrons in an unbalanced configuration. The applied sputter power density was 3.0 W/cm^2. The substrate was located off-axis from the target normal, reducing the impact of high energetic ions. The total deposition pressure was 0.6 Pa measured by a capacitance manometer. Hydrogen doping was achieved by injecting deionized water vapor through a needle valve or H_2 gas via a mass flow controller. In the case of H_2O, the O_2 flow was optimized for each H_2O dose in order to achieve minimum resistivity, since both gases, O_2 and H_2O, affect the IOH stoichiometry. As H_2O makes out the major part of the background gas, the H_2O partial pressure includes the base pressure too. Injection of H_2O vapor through a needle valve directly from a liquid water reservoir might pose a challenge for industrial applications since in practice it needs some time until the partial pressure is stabilized. Therefore, a highly controllable way to inject hydrogen was achieved by a commercial MFC using H_2 gas. In order to exclude doping from water vapor, which to some extent is always present, the base pressure for H_2 experiments was always below 9.8×10^{-6} Pa. The presented O_2/H_2 partial pressures were calculated from relative gas flows.

The film thickness was determined by stylus profilometry. Hall measurements were performed at room temperature with an Ecopia HMS 3000 system in the Van der Pauw geometry. X-ray diffraction (XRD) patterns were recorded in the Bragg-Brentano configuration using a Bruker D8 Discover diffractometer operating with the CuK_α radiation.

Film stoichiometry was determined by Rutherford backscattering spectrometry (RBS) performed with a 2 MeV ^{4}He beam and a silicon PIN diode detector under 168°. The collected data were simulated using the RUMP software.[29] Hydrogen concentration depth profiles were measured by elastic recoil detection analysis (ERDA) using a 2 MeV ^{4}He beam with an incidence angle of 15° towards the sample surface and a Si surface barrier detector with absorber foil at a forward scattering angle of 30°.

Optical transmittance and reflectance were measured using a Shimadzu UV-3600 spectrophotometer with an integrating sphere. The optical absorptance A was calculated from the relation $A = 1\text{-}T\text{-}R$. Optical data of the TCOs are given for the whole layer/1-mm-glass stack. The morphology was studied by scanning electron microscopy (SEM) on a Hitachi microscope with an accelerating voltage of 5.0 keV.

Thin film Cu(In,Ga)Se_2 absorbers were deposited on Mo coated soda lime glass in a 3-stage co-evaporation process.[5] The absorbers presented in Sec. III B were fabricated with a composition of $[Cu]/[In + Ga] = 0.85$ and $[Ga]/[In + Ga] = 0.42$, whereas for the stability tests in Sec. III C, a different batch of absorbers with a composition of $[Cu]/[In + Ga] = 0.83$ and $[Ga]/[In + Ga] = 0.41$ was used. For each absorber, a NaF post-deposition treatment (PDT) was carried out *in-situ*.[5] CdS buffer layer was grown by chemical bath deposition and the *n*-type part of the photovoltaic devices were completed by sputter-depositing first 70 nm of intrinsic ZnO (i-ZnO) followed by sputtering for a necessary thickness of IOH and AZO. The reference front electrode was sputter-deposited in a vacuum chamber with a direct facing target optimized for highest opto-electrical properties for AZO grown without intentional heating. Ceramic $ZnO:Al_2O_3$ (98:2 wt. %, purity 99.995%) targets with a diameter of 10.16 cm (4 in.) were sputtered in a mixed Ar/O_2 atmosphere with a total pressure of 0.15 Pa and a power density of 2.5 W/cm^2. The solar cells were finished with a Ni/Al/Ni grid by electron-beam deposition. For all the presented experiments, no anti-reflection coatings were applied to the cells.

The PV parameters of the solar cells were measured under simulated standard-test conditions (1000 W m^{-2}, AM 1.5 G illumination, 25 °C) using a sun-simulator from LOT-Oriel. Current density-voltage (*J-V*) curves were acquired with a Keithley 2400 source meter and four-terminal sensing. The external quantum efficiency (*EQE*) was determined with a lock-in amplifier using a probe beam from a chopped white light source (900 W, halogen lamp, 360 Hz) passing a dual grating monochromator. The beam spot covered the area between the outer metal grid fingers, and, for obtaining the absolute *EQE* value, a certified monocrystalline Si solar cell from Fraunhofer ISE was used as reference.

Stability tests of heat-light soaking (HLS) for 500 h were performed at 80 °C and 500 mbar of dry air. White light-emitting diodes were used as the illumination source, and the intensity was adjusted such that the J_{SC} measured *in-situ* was the same as determined with the sun-simulator under simulated standard-test conditions. Relative changes of the PV parameters were recorded *in-situ*.

III. RESULTS AND DISCUSSION

A. Hydrogen doping of In_2O_3

Electrical properties of In_2O_3 thin films doped by the injection of H_2O vapor are depicted in Fig. 1(a). Already a small amount of water vapor of 1.3×10^{-5} Pa, which is only provided by the background gas, is sufficient to dope In_2O_3 with H to an electron density $>10^{20}$ cm^{-3}. The doping density stays in the range of $3.6\text{–}5.2 \times 10^{20}$ cm^{-3} for H_2O vapor pressure between 7×10^{-5} and 10^{-3} Pa. The electron mobility decreases from ~50 to 28 cm^2/Vs in this range causing the resistivity to increase again for too large H_2O vapor pressures. The high mobility values are equal to those previously reported hydrogenated In_2O_3 of 50 cm^2/Vs at a carrier density of $3\text{–}4 \times 10^{20}$ cm^{-3}.[17,26]

Fig. 1(b) shows the successful hydrogen doping of In_2O_3 by injection of H_2 gas. The ratio of oxygen to the total flow was kept constant at 1.0%. For H_2 partial pressures larger than 1.4 mPa, the achieved doping concentration is already in the low 10^{20} cm^{-3} region. An electron mobility of 55 cm^2/Vs is observed for H_2 doped samples, as high as for IOH films doped via H_2O vapor. For both doping methods, the electron mobility decreases for higher H_2O/H_2 partial pressures and depends roughly linear on the inverse carrier density suggesting ionized impurity scattering as the main limiting factor for electron transport.[30] Koida *et al.* found that the optical mobility of IOH thin films determined from spectroscopic ellipsometry is almost equal to the mobility measured by Hall indicating that these scattering events occur within the amorphous matrix.[19]

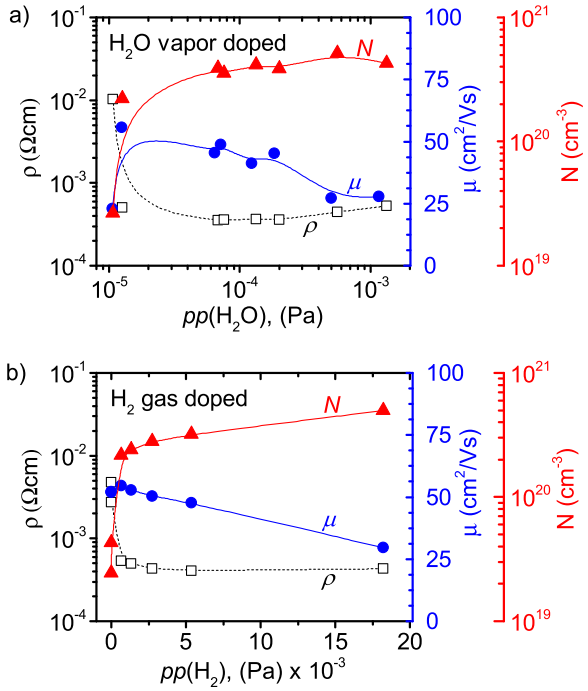

FIG. 1. Electrical properties, determined from Hall measurements, of In_2O_3 with injection of (a) H_2O vapor and (b) H_2 during the sputter-deposition. Solid lines are for guiding the eye only.

Indium oxide grows poly-crystalline even when sputter-deposited without intentional heating.[17] The injection of H_2O vapor or H_2 yields, in both cases, the amorphous structure (Fig. 2). Koida and Kondo suggested that the formation of In–OH bonds prevents the consecutive network of In–O–In bonds.[17] This explanation would also be consistent in the case of H_2 gas doping, where OH fragments can easily form in the plasma or after adsorption on the growing film surface. In contrast, the as-deposited reference AZO films are crystalline at room temperature, exhibiting a columnar growth with a preferential orientation along the c-axis.

ERDA measurements were performed for depth profiling of the hydrogen content (Fig. 3). A peculiarity of ERDA is that a constant bulk dopant concentration results in a decreasing signal with increasing probe depth, due to the change of energy and energy loss of the He projectiles and H recoils. In order to represent this dependence, a standard

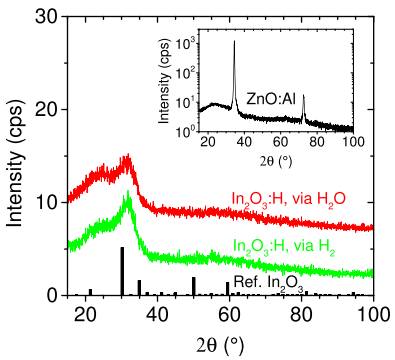

FIG. 2. X-ray defraction patterns of In_2O_3:H doped via H_2O or H_2, and reference In_2O_3 powder. (Inset) XRD pattern of ZnO:Al displaying the (002) and (004) plane.

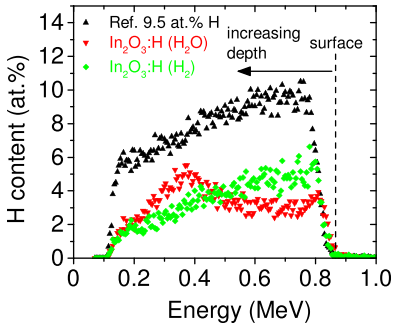

FIG. 3. ERDA measurements showing hydrogen depth profiles of the 9.5 at. % standard sample (mica), IOH films doped via H_2O vapor (0.8% O_2 flow, $pp(H_2O) = 6.75 \times 10^{-5}$ Pa), and H_2 gas (1.0% O_2, and 1.0% H_2 flow).

material (mica) with a constant 9.5 at. % hydrogen content has been added to the depth-profile for comparison. The film surface is visible in the spectra as the signal onset at the recoil energy of 0.85 MeV. IOH films doped by H_2O vapor exhibit a nonconstant hydrogen incorporation with a maximum concentration in the first half of the deposition. The H gradient is present even though the opening of the needle valve was constant. The origin of the gradient is unclear; one cannot exclude that water is outgassing from chamber walls, sputter chimneys, and other holders due to heating by the plasma. The total H content was estimated by integrating the ERDA signal and scaling with the 9.5 at. % standard. The total bulk concentrations were found to be 4.1 and 4.4 at. % H for H_2O and H_2, respectively.

The optical performance of the TCOs is normally compared in terms of their optical absorptance (Fig. 4). The optical absorbance and electrical properties of the TCOs are fundamentally interlinked, and therefore, Hall data of these samples are given in Table I to highlight their optical-electronic correlation. The ultraviolet (UV) cut-off of AZO thin films occurs at a shorter wavelength than for both IOH samples due to a wider band gap and a slightly higher carrier density as a result of the Burstein-Moss shift. Comparing two different doping methods, the optical band gap is lower for indium oxide films doped with H_2. This is in agreement with the lower carrier density in the thicker IOH (H_2) layer (Table I), although the lower optical bandgap can also be induced by a different degree of the lattice disorder in the amorphous material. We have chosen TCOs with equal sheet resistance and therefore different thickness in view of their

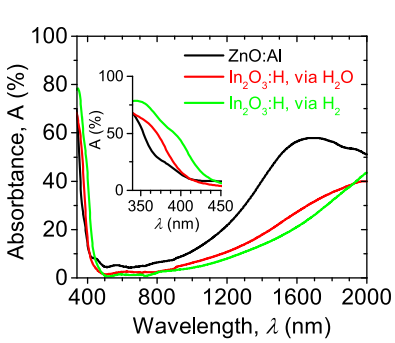

FIG. 4. Optical absorptance $A = 1\text{-}T\text{-}R$ of AZO, and IOH via H_2O and H_2 including the whole TCO/glass stack. (Inset) Zoom in of absorptance A displaying the absorption edge.

TABLE I. Sputter parameters and electrical properties of the implemented TCOs.

	ZnO:Al	In_2O_3:H (H_2O)	In_2O_3:H (H_2)
$pp(O_2)$, (Pa)	7.2×10^{-5}	4.4×10^{-3}	5.4×10^{-3}
$pp(H_2/H_2O)$, (Pa)	—	8.9×10^{-5}	1.4×10^{-3}
ρ (Ω cm)	5.2×10^{-4}	4.0×10^{-4}	5.6×10^{-4}
N (cm^{-3})	4.4×10^{20}	3.3×10^{20}	2.3×10^{20}
μ ($cm^2\ V^{-1}\ s^{-1}$)	27	47	48
Thickness, d (nm)	460	330	440

implementation in solar cells. The absorption of both IOH samples is almost equal in the visible region and significantly lower than the reference AZO. The gain in optical performance of IOH films compared to AZO is more pronounced in the IR region above 700 nm. From classical Drude theory, the plasma frequency is given as[15]

$$\omega_p = \sqrt{\frac{ne^2}{m^* \varepsilon_\infty \varepsilon_0}}, \quad (1)$$

where n is the carrier density, e is the elementary charge, m^* is the effective mass, and $\varepsilon_\infty\varepsilon_0$ is the permittivity of the material. For AZO, the plasma wavelength $\lambda_p = 2\pi c/\omega_p$ occurs at $\sim$1.7 μm, whereas for In_2O_3:H films, λ_p is shifted towards higher wavelengths not covered by the spectrometer. From Eq. (1) and the carrier density from Table I, the plasma wavelength of In_2O_3:H films are expected to be at 2.3 μm (via H_2O) and 2.8 μm (via H_2) assuming an effective mass of $0.373 \cdot m_0$ and a permittivity of $4.26 \cdot \varepsilon_0$,[19] where m_0 is the electron mass and ε_0 is the vacuum permittivity. The higher mobility of IOH films allows a lower doping concentration for equal conductance, and therefore, an enhanced optical transmission of solar energy is possible particularly in the IR region.

B. Implementation in CIGS solar cells

Recent world record efficiencies of CIGS solar cells have all been achieved with AZO front contacts.[1–5] Therefore, we compare hydrogenated In_2O_3 implemented as front electrode in CIGS devices with AZO as reference. Table I lists electrical properties of the optimized IOH and AZO contacts, which were first deposited on flat glass substrates in order to exclude the effect of substrate roughness and conductivity. The thickness of all three TCOs was adjusted to yield the same sheet resistance of $\sim$12 $\Omega/\square$ on bare glass in order to exclude effects of series resistivity on the cell fill factor FF and open circuit voltage V_{OC}. It should be noted that the mobility of the TCO films on the rough CIGS absorbers is lower than on flat glass. Using four gold contacts evaporated onto the finished cell (without metal grid), the mobility of IOH (H_2O) was measured to be $\sim$13 cm^2/Vs as compared to 47 cm^2/Vs for the flat glass.

Cross section and top view SEM pictures of finished devices with AZO and IOH (via H_2O doping) front contacts are displayed in Fig. 5. The columnar growth of AZO films in CIGS devices with a rather small diameter is shown in Figs. 5(a) and 5(c). Uniform coverage seems to be achieved with IOH films in the cross section view of Fig. 5(b), but the top view in Fig. 5(d) reveals that voids separate the layer grains.

Current–voltage data and *EQE* curves of the best solar cells are depicted in Fig. 6, whereas PV parameters of nine cells are depicted in Fig. 7 for all three cases. The first prominent feature of the IOH devices is an enhanced average V_{OC} of +18 and +23 mV for H_2O and H_2 doping, respectively. The improved V_{OC} was reproduced on many CIGS absorbers with different metal ratios.

An important factor that could influence the V_{OC} of CIGS solar cells is the temperature during the various deposition steps. The only variation of the investigated devices is the sputter-deposition of the TCOs and apart from that step the same deposition batch was used. No intentional heating was applied during sputtering for either case, and therefore, the influence of deposition temperature can safely be discarded. The hole density in the p-type CIGS is also decisive for the V_{OC}, but should be constant for the same process batch. Recombination losses are the main limiting factor for the V_{OC} in CIGS solar cells which are heavily influenced by defect states. Hydrogenated In_2O_3 grows in the amorphous state with very high opto-electrical properties even at room temperature, and no assisted ion flux is needed. The sputter-deposition condition of IOH was therefore very mild with no significant bombardment of ions with energy >100 eV, which is often the case for sputtering direct facing targets with high electronegative elements. In contrast, the solar cells were under direct influence of high energy O^- ions when depositing AZO. Therefore, we propose that the introduction of IOH front contacts reduces the recombination current due to an improved i-ZnO/IOH interface and by a beneficial work function offset.

The average J_{SC} exhibits 31 mA/cm^2 for the AZO and IOH (H_2O) devices and a lower value of 30 mA/cm^2 for the IOH (H_2) device. This decrease is caused by a lower optical band gap of the IOH (H_2) film (see Fig. 4) yielding a reduced photon collection of the absorber in the UV region which is also visible in a lower *EQE* in Fig. 6(b). Because of the

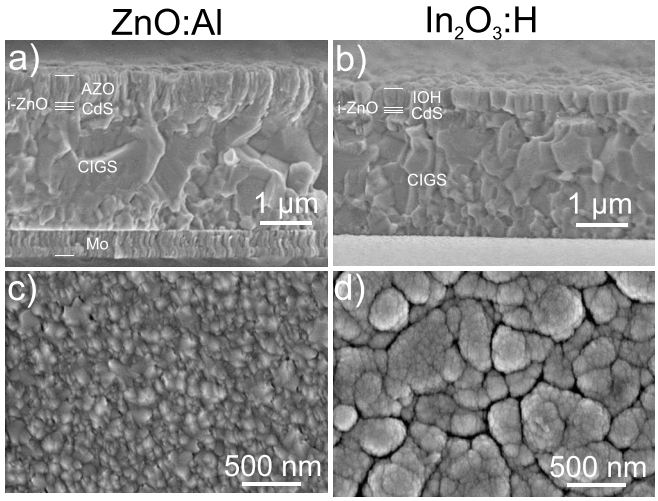

FIG. 5. SEM cross section and top view pictures of finished devices with ZnO:Al ((a) and (c)) and In_2O_3:H via H_2O doping ((b) and (d)) front contacts.

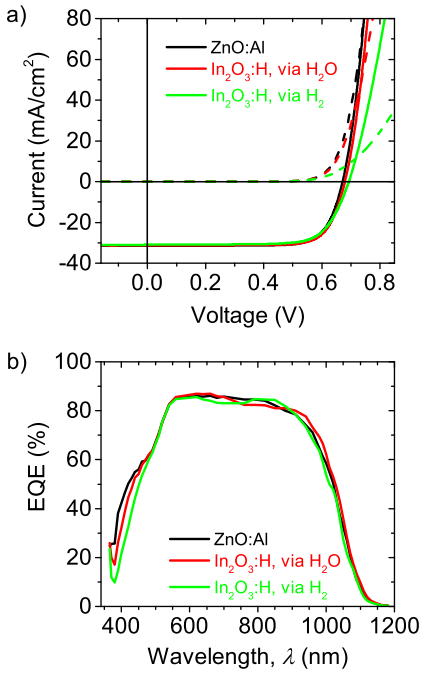

FIG. 6. (a) Current–voltage *J-V* and (b) external quantum efficiency *EQE* data of the record CIGS cells with AZO, IOH (H_2O), and IOH (H_2) front contacts.

absorber band gap of ∼1.16 eV, the *EQE* ends at 1.1 μm and the superior performance of the IOH films in the near infrared (NIR) region does not contribute to a higher J_{SC}.

The average fill factor *FF* of the IOH (H_2O) devices is 76%, slightly higher compared to the reference AZO device, which marks its successful implementation in CIGS solar cells with a sufficiently low series and high parallel resistance. In contrast, the IOH (H_2) cells suffer from an average *FF* loss of 4% in Fig. 6(a). This implies a higher cell series resistance corresponding to increased charge carrier scattering either at the i-ZnO/IOH or the IOH/grid interface as the device structure is otherwise the same. One possibility is that the reactive gas H_2, or radicals thereof, can change the i-ZnO/IOH creating a high resistive interlayer. Another scenario is a high contact resistance to the metal grid which was observed by Barraud *et al.* for H_2O doped In_2O_3.[26]

Overall the efficiency η could be improved from 15.7% to 16.2% by substituting IOH (H_2O) for AZO as front contacts mainly due to a higher V_{OC} of ∼20 mV.

C. Stability test under heat-light soaking

As an initial stability test, several CIGS solar cells with AZO (180 nm, 85 Ω/□) and IOH (H_2O doped, 330/200 nm, 54/73 Ω/□) front contacts were treated under heat-light soaking for 540 h at 80 °C and 500 mbar dry air. The effect of humidity is beyond the scope of this work. The cells were not encapsulated, and the PV parameters were measured *in-situ* each 30 min.

The maximum power (P_{MPP}) changes only by +4% for the IOH (H_2O) devices demonstrating their high potential for long term stability, whereas the AZO cell degrades by relative −8% under chosen heat-light conditions Fig. 8(a). In the following, the origin of the P_{MPP} characteristics is discussed in terms of the J_{SC}, V_{OC}, and the *FF* depicted in Figs. 8(b) and 8(c).

Within the first 50 h, a rather steep increase of the J_{SC} is observed for all tested samples, which is followed by a constant value for the IOH (54 Ω/□), and the AZO device while

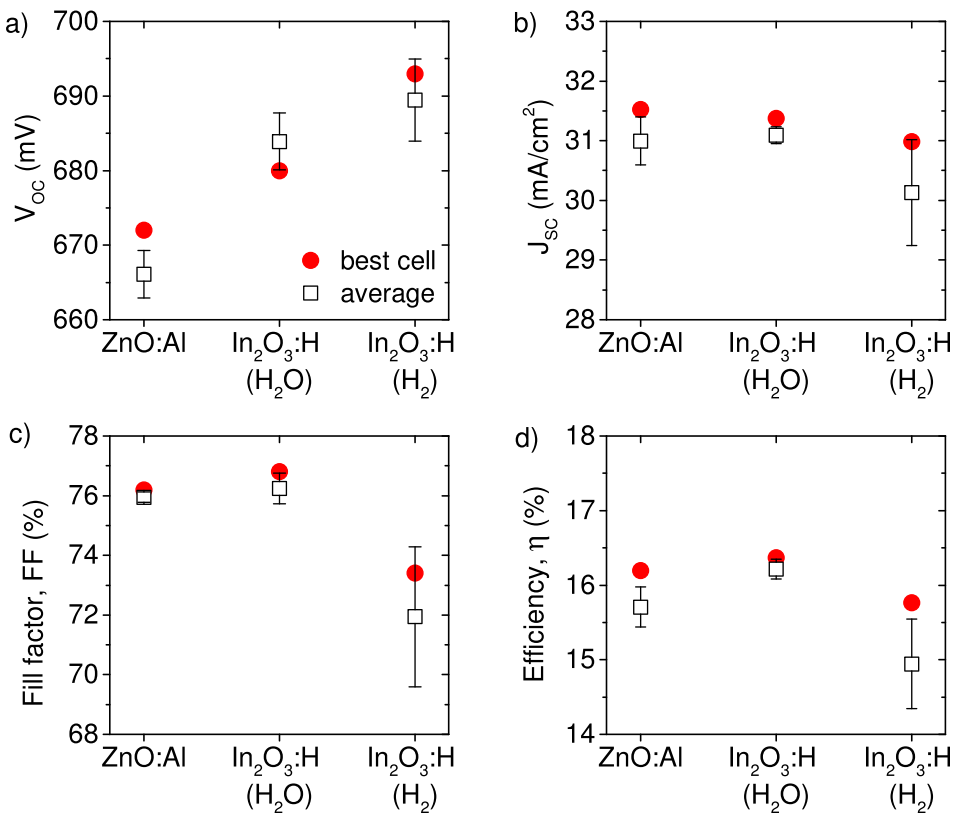

FIG. 7. Photovoltaic parameters of CIGS solar cells with AZO, IOH (H_2O), and IOH (H_2) front contacts for the best cell and an average value for nine cells. The cell area was 0.3 cm^2 for all devices.

the IOH (73 Ω/□) cell shows a monotonic increase. Regarding the different behavior of the IOH (54 Ω/□) and IOH (73 Ω/□) devices after 50 h, we emphasize that the only parameter that distinguishes them is the sputter time during the TCO deposition, but the origin remains unclear.

For all samples, the V_{OC} improved slightly within the first 100 h but then stays stable for over 400 h. An increase in V_{OC} under illumination and forward bias has been measured in $CuInSe_2$ based solar cells,[31,32] which can be caused by metastable defect states[33,34] such as V_{Se}-V_{Cu} divacancies observed in CIGS solar cells.[35,36] Once the cells are taken out of the stress chamber, the V_{OC} relaxes approaching initial values as measured on the solar simulator before the stability test.

The degradation of the AZO cell can be solely ascribed to a continuous loss of the *FF*. To elucidate the *FF* loss of the AZO device, the electron mobility of this cell, including the metal grid, was determined by Hall measurements in the Van der Pauw geometry with the probe tips placed directly onto the TCO. The resulting value of 6 cm^2/Vs marks a significant reduction compared to as-deposited AZO films on glass with a mobility of ~25 cm^2/Vs. Mobility loss of AZO under damp heat exposure has been observed especially for thin films <220 nm.[37] Greiner *et al.* investigated the damp heat stability of AZO films on various substrates with different degrees of roughness and traced the mobility loss back to local perturbations of the AZO growth.[38] These so called extended grain boundaries (eGBs) occur preferentially at edges and troughs, thus hindering the electronic transport after damp heat treatments especially for rough substrates. In our case, the cells were treated only under increased heat exposure, but the evident decrease of mobility and a rough CIGS surface make the degradation mechanism via eGBs very plausible. For amorphous TCOs, such eGBs are not expected. Indeed, an excellent stability of amorphous TCOs, such as a-InZnO,[12] has been shown under damp heat tests.

IV. SUMMARY AND CONCLUSIONS

Two different hydrogen doping methods of indium oxide based TCOs and their implementation in solar cells have been investigated. The injection of hydrogen has been achieved by adding water vapor or hydrogen gas during the sputter process yielding in both methods a carrier concentration of $>3 \times 10^{20}$ cm^{-3} and caused the film to grow with an amorphous structure. The electron mobility of IOH films via H_2O vapor and H_2 doping exhibits exceptionally high values of ~50 cm^2/Vs for films grown without intentional heating, which is comparable to the highest reported values.[17,26] An excess amount of H during the sputter-deposition results in a decrease of the mobility due to ionized impurity scattering. The dependence of hydrogen partial pressure on the doping concentration is relatively small when the film is doped with H_2O vapor in contrast to H_2, where the carrier concentration increases roughly linear with the H_2 partial pressure for films in the degenerate state. The high mobility and relatively low carrier concentration of IOH films doped via H_2O vapor or H_2 give excellent optical properties with low optical absorption in the visible region with a plasma frequency >2.3 μm making them ideal candidates as transparent front contacts in solar cells.

IOH films have been successfully implemented as front contacts in CIGS solar cells then compared to state-of-art AZO based devices. Contrary to previous reports,[28] no gain in J_{SC} has been observed for as-deposited IOH front contacts in CIGS solar cells. Even though the optical absorption of

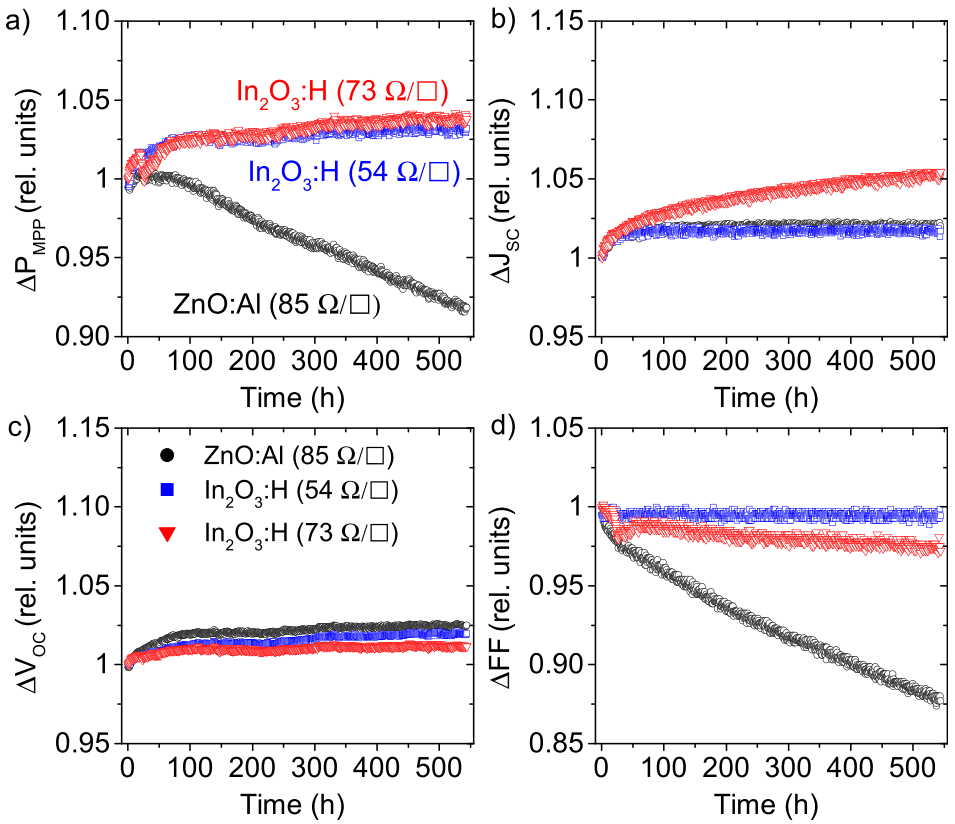

FIG. 8. *In-situ* measured PV parameters showing relative changes of maximum power P_{MPP}, J_{SC}, V_{OC}, and *FF* during HLS for >500 h at 80 °C, and 500 mbar dry air. All cells were not encapsulated with the initial TCO sheet resistance given in the brackets.

IOH films is lower in the region >500 nm, the J_{SC} remains constant compared to AZO in our case, due to a lower optical band gap in IOH and the absorber band gap of 1.16 eV that limits the IR spectral response. The high IR optical performance of as-deposited IOH front contacts seems to be more suitable for low band gap absorbers such as $CuInSe_2$ and $Cu_2ZnSn(S,Se)_4$, or in multi-junction solar cells.

Most importantly, the open circuit voltage V_{OC} of IOH-containing CIGS solar cells could be enhanced on average by ~18 mV and ~23 mV for H_2O and H_2 doping of IOH, respectively, as compared to reference AZO electrodes. The IOH electrodes are different to AZO not only in their higher electron mobility but also they are of the amorphous structure, exhibit a higher work function, and are deposited under conditions with a reduced O^- ion bombardment. We suggest that the lower recombination current yielding the enhanced V_{OC} is caused by the improved i-ZnO/IOH interface due to the decreased ion bombardment resulting in a lower defect density in the i-ZnO layer, in combination with more beneficial band offset at this interface, which is investigated in more details in Ref. 39. In total, the average power conversion efficiency can be enhanced by absolute 0.5% to 16.2% when implementing the IOH (via H_2O) front contacts. Finally, stability tests under heat-light soaking exhibit an improved stability of CIGS cells with the new electrodes, which is important for eventual implementation in large-scale PV modules. Our results demonstrate the prospect of the amorphous IOH for long-term implementation in CIGS solar cells, although further combined damp heat tests will be needed.

ACKNOWLEDGMENTS

The authors would like to thank Till Coester for technical support. Proofreading by Michael Rawlence is gratefully acknowledged. The work was supported by Competence Center Energy and Mobility (CCEM) under the project CONNECT-PV.

[1]P. Jackson, D. Hariskos, R. Wuerz, O. Kiowski, A. Bauer, T. M. Friedlmeier, and M. Powalla, Phys. Status Solidi RRL **9**, 28 (2015).
[2]P. Reinhard, A. Chirila, P. Blosch, F. Pianezzi, S. Nishiwaki, S. Buechelers, and A. N. Tiwari, IEEE J. Photovoltaics **3**, 572 (2013).
[3]A. Chirilă, P. Reinhard, F. Pianezzi, P. Bloesch, A. R. Uhl, C. Fella, L. Kranz, D. Keller, C. Gretener, H. Hagendorfer, D. Jaeger, R. Erni, S. Nishiwaki, S. Buecheler, and A. N. Tiwari, Nat. Mater. **12**, 1107 (2013).
[4]P. Jackson, D. Hariskos, E. Lotter, S. Paetel, R. Wuerz, R. Menner, W. Wischmann, and M. Powalla, Prog. Photovoltaics **19**, 894 (2011).
[5]A. Chirila, S. Buecheler, F. Pianezzi, P. Bloesch, C. Gretener, A. R. Uhl, C. Fella, L. Kranz, J. Perrenoud, S. Seyrling, R. Verma, S. Nishiwaki, Y. E. Romanyuk, G. Bilger, and A. N. Tiwari, Nat. Mater. **10**, 857 (2011).
[6]F. Pianezzi, Ph.D. dissertation, ETH Zürich, 2014.
[7]D.-W. Lee, W.-J. Cho, J.-K. Song, O.-Y. Kwon, W.-H. Lee, C.-H. Park, K.-E. Park, H. Lee, and Y.-N. Kim, "Failure analysis of $Cu(In,Ga)Se_2$ photovoltaic modules: degradation mechanism of $Cu(In,Ga)Se_2$ solar cells under harsh environmental conditions," Prog. Photovoltaics (published online).
[8]T. Minemoto and J. Julayhi, Curr. Appl. Phys. **13**, 103 (2013).
[9]Y. Kuwahata and T. Minemoto, Renewable Energy **65**, 113 (2014).
[10]A. E. Delahoy, L. Chen, M. Akhtar, B. Sang, and S. Guo, Sol. Energy **77**, 785 (2004).
[11]C. P. Thompson, S. Hegedus, P. Carcia, and R. S. McLean, IEEE J. Photovoltaics **3**, 494 (2013).
[12]J. D. Perkins, T. Gennett, J. E. Leisch, R. Sundaramoorthy, I. L. Repins, M. F. A. M. van Hest, and D. S. Ginley, "Amorphous transparent conductors for PV applications," in *2010, 35th IEEE Photovoltaic Specialists Conference (PVSC), Honolulu, HI* (IEEE, Piscataway, NJ, 2010), pp. 000989–000991.
[13]T. Gennett, J. D. Perkins, I. L. Repins, R. Sundaramoorthy, and D. S. Ginley, "The stability and performance of amorphous-InZnO within CIGS devices," Proc. SPIE **7771**, 77710O (2010).
[14]K. Nomura, H. Ohta, A. Takagi, T. Kamiya, M. Hirano, and H. Hosono, Nature **432**, 488 (2004).
[15]D. Ginley, H. Hosono, and D. C. Paine, *Handbook of Transparent Conductors* (Springer, 2011).
[16]J. S. Park, W.-J. Maeng, H.-S. Kim, and J.-S. Park, Thin Solid Films **520**, 1679 (2012).
[17]H. F. T. Koida and M. Kondo, Jpn. J. Appl. Phys. **46**, L685 (2007).
[18]M. P. Taylor, D. W. Readey, M. F. A. M. van Hest, C. W. Teplin, J. L. Alleman, M. S. Dabney, L. M. Gedvilas, B. M. Keyes, B. To, J. D. Perkins, and D. S. Ginley, Adv. Funct. Mater. **18**, 3169 (2008).
[19]T. Koida, M. Kondo, K. Tsutsumi, A. Sakaguchi, M. Suzuki, and H. Fujiwara, J. Appl. Phys. **107**, 033514 (2010).
[20]T. Koida, H. Shibata, M. Kondo, K. Tsutsumi, A. Sakaguchi, M. Suzuki, and H. Fujiwara, J. Appl. Phys. **111**, 063721 (2012).
[21]S. Lany and A. Zunger, Phys. Rev. Lett. **98**, 045501 (2007).
[22]S. Limpijumnong, P. Reunchan, A. Janotti, and C. Van de Walle, Phys. Rev. B **80**, 193202 (2009).
[23]P. King, R. Lichti, Y. Celebi, J. Gil, R. Vilão, H. Alberto, J. Piroto Duarte, D. Payne, R. Egdell, I. McKenzie, C. McConville, S. Cox, and T. Veal, Phys. Rev. B **80**, 081201(R) (2009).
[24]T. Koida, H. Sai, and M. Kondo, Thin Solid Films **518**, 2930 (2010).
[25]H. Scherg-Kurmes, S. Körner, S. Ring, M. Klaus, L. Korte, F. Ruske, R. Schlatmann, B. Rech, and B. Szyszka, Thin Solid Films (published online).
[26]L. Barraud, Z. C. Holman, N. Badel, P. Reiss, A. Descoeudres, C. Battaglia, S. De Wolf, and C. Ballif, Sol. Energy Mater. Sol. Cells **115**, 151 (2013).
[27]C. Battaglia, L. Erni, M. Boccard, L. Barraud, J. Escarré, K. Söderström, G. Bugnon, A. Billet, L. Ding, M. Despeisse, F.-J. Haug, S. D. Wolf, and C. Ballif, J. Appl. Phys. **109**, 114501 (2011).
[28]S. K. H. Scherg-Kurmes, F. Ruske, C. Wolf, R. Muydinov, R. Schlatmann, and B. Szyszka, in *High Mobility InOx:H Transparent Conductive Oxide for Thin Film Solar Cells, Dresden, Germany* (ICCG 10) (2014), p. 381.
[29]L. R. Doolittle, Nucl. Instrum. Methods Phys. Res. Sect. B **15**, 227 (1986).
[30]D. H. Zhang and H. L. Ma, Appl. Phys. A **62**, 487 (1996).
[31]M. N. Ruberto and A. Rothwarf, J. Appl. Phys. **61**, 4662 (1987).
[32]U. Rau and H. W. Schock, Appl. Phys. A **69**, 131 (1999).
[33]M. Igalson and H. W. Schock, J. Appl. Phys. **80**, 5765 (1996).
[34]U. Rau, M. Schmitt, J. Parisi, W. Riedl, and F. Karg, Appl. Phys. Lett. **73**, 223 (1998).
[35]M. Cwil, M. Igalson, P. Zabierowski, and S. Siebentritt, J. Appl. Phys. **103**, 063701 (2008).
[36]M. Igalson, A. Urbaniak, A. Krysztopa, Y. Aida, R. Caballero, M. Edoff, and S. Siebentritt, Thin Solid Films **519**, 7489 (2011).
[37]F. J. Pern, S. H. Glick, X. Li, C. DeHart, T. Gennett, M. Contreras, and T. Gessert, "Stability of TCO window layers for thin-film CIGS solar cells upon damp heat exposures: Part III," Proc. SPIE **7412**, 74120K (2009).
[38]D. Greiner, S. E. Gledhill, C. Köble, J. Krammer, and R. Klenk, Thin Solid Films **520**, 1285 (2011).
[39]T. Jäger, Y. E. Romanyuk, B. Bissig, F. Pianezzi, S. Nishiwaki, P. Reinhard, J. Steinhauser, J. Schwenk, and A. N. Tiwari, "Improved open-circuit voltage in $Cu(In,Ga)Se_2$ solar cells with high work function transparent electrodes," J. Appl. Phys. (submitted).